

# MODEL SPECTRA OF ROTATION POWERED PULSARS IN THE INTEGRAL RANGE

J. Dyks<sup>1</sup>, B. Rudak<sup>1,2</sup>, and T. Bulik<sup>3</sup>

<sup>1</sup>Nicolaus Copernicus Astronomical Center, Toruń, Poland

<sup>2</sup>TCfA of Nicolaus Copernicus University, Toruń, Poland

<sup>3</sup>Nicolaus Copernicus Astronomical Center, Warsaw, Poland

## ABSTRACT

The energy range of IBIS is a promising ground for testing mutual relations of distinct components expected in the spectra of high-energy radiation from rotation powered pulsars. According to some polar-cap models two such components - due to curvature and synchrotron emission - may contribute comparable amounts of power between 15 keV and 10 MeV (Rudak & Dyks, 1999). Zhang & Harding (2000) argued recently for the inclusion of a third possible component, due to inverse Compton scattering (ICS) of soft thermal photons on secondary  $e^\pm$ -pairs. Here we present the results of Monte Carlo calculations of all three spectral components within a polar-cap model which allows for interactions of relativistic particles with the soft photons coming from the pulsar surface. For teragauss pulsars with the surface temperature of a few  $\times 10^5$  K the ICS component dominates the spectrum in the energy range below 10 MeV, and thus its presence increases the ratio of X-ray to  $\gamma$ -ray luminosity (in comparison to the models ignoring the ICS on secondary  $e^\pm$ -pairs) to a level observed in the Vela pulsar.

Key words: radiation processes: non-thermal; stars: neutron; pulsars: general.

## 1. INTRODUCTION

The standard polar cap model of pulsars refers to the pair-photon cascades induced by photons of curvature radiation (CR) due to ultrarelativistic electrons leaving the neutron star (NS) surface (primary particles). Although successful in reproducing gamma-ray spectra observed above 100 MeV (Daugherty & Harding, 1982) the model fails to reproduce the relative level of X-ray and gamma-ray emission. As shown by Zhang & Harding (2000) this might be caused by neglecting the resonant inverse Compton scattering (ICS) of thermal photons from the surface by the secondary  $e^\pm$  pairs. The authors developed an approximate analytical method to model the X-ray

luminosities (with the ICS contribution included) of pulsars detected by ROSAT and ASCA. Their results indicate that in terms of power in the X-ray range the ICS component may be competitive to both the curvature and synchrotron components. However, in order to verify the conclusion of Zhang & Harding (2000), and to obtain detailed spectra the Monte Carlo simulations are necessary.

In this work we present basic features of such Monte Carlo spectra for different pulsar parameters. In particular, the role and properties of the spectral component due to resonant inverse Compton scattering on secondary  $e^\pm$ -pairs are addressed. We find that the shape and the strength of this component are sensitive to the strength of the local magnetic field as well as to the size and temperature of the thermal source.

## 2. THE MODEL

As a starting point we took a model of high-energy processes in pulsar magnetospheres as proposed by Daugherty & Harding (1982). The model was then furnished with a modern version of a strong electric field  $E_\parallel$  after Harding & Muslimov (1998) with the lower, and the upper boundary of the accelerator at the height  $h_0$ , and  $h_c$  above the stellar surface, respectively. In each case the size of acceleration zone  $h_c - h_0$  was determined selfconsistently in the course of calculations. An extended source of soft thermal photons located on the pulsar surface has been added (see below for details). Primary electrons slide along open dipolar lines of the magnetic field and attain ultrarelativistic energies in the presence of this field. At the same time they loose the energy via two processes: curvature radiation (CR) and inverse Compton scattering (ICS). Due to a large strength of the  $E_\parallel$ , the former process dominates the cooling of the electrons. In consequence, vast majority of electromagnetic cascades is induced by curvature photons and very few by ICS (upscattered soft) photons. This allows us to ignore any ICS-induced cascades and to model the cascades in the following way:

First, the CR-induced cascade of  $e^\pm$  pairs and synchrotron photons is simulated following Rudak & Dyks (1999). The primary electrons are accelerated along the last open lines of purely dipolar magnetic field and emit curvature photons. Some of these photons undergo one-photon magnetic absorption producing  $e^\pm$  pairs. The pairs emit in turn synchrotron photons (SR) which also may produce higher generations of  $e^\pm$  pairs with their own SR photons, etc..

In the second step, the simulation of the resonant ICS for the  $e^\pm$  pairs proceeds after Dyks & Rudak (2000). Three different cases for the source of thermal photons are considered: **A**) a hot cap of temperature  $T_{\text{hot}} \simeq$  a few  $\times 10^6$  K and radius  $R_{\text{hot}} \simeq 10^5$  cm centered on the magnetic pole; **B**) entire neutron star surface with  $T_{\text{surf}} \simeq$  a few  $\times 10^5$ ; **C**) the hot cap of **A**) with the rest of the surface at  $T = 5 \cdot 10^5$  K. In order to simplify the calculations of scatterings in the cases **A**) and **C**) (with the hot cap) we made the following axial geometry approximation: for the local ambient soft photon field as seen by a  $e^\pm$ -pair we took a field that would be seen if the pair were moving along the dipole axis at the same radial coordinate.

For the sake of completeness the ICS component due to the primary electrons is calculated in the last step, even though this component is not important energetically.

We would like to emphasize that the numerical code constructed for this model does not follow the directional pattern of the outgoing radiation. It calculates a ‘single particle’ spectrum of a pulsar, ie. the spectrum due to a single primary electron accelerated to an ultrarelativistic energy in the presence of a strong electric field. In this sense our work should be considered as a first approximation in modelling phase-averaged spectra.

### 3. RESULTS

Fig.1 shows the spectrum calculated for a pulsar with  $B_{\text{pc}} = 6$  TG,  $P = 0.1$  s (the parameters close to those of the Vela or B1706–44) and a hot cap with  $R_{\text{hot}} = 10^5$  cm and  $T_{\text{hot}} = 5 \cdot 10^6$  K. The total spectrum (thick solid line) is a sum of three components: the curvature spectrum (dot-dashed line), the synchrotron spectrum emitted by the  $e^\pm$  pairs (short dashed line), and the inverse Compton spectrum of photons scattered by the  $e^\pm$  pairs (thin solid line). The fourth spectral component – the inverse Compton spectrum of photons upscattered by the primary electron – shown as the long dashed line is never energetically important. This is because the primary undergoes a strong acceleration and its energy increases quickly above the value required to fulfill the resonant condition. For this reason we have also ignored any magnetic absorption of these ICS photons and the subsequent creation of  $e^\pm$ -pairs. At the same time the ICS component due to the  $e^\pm$  pairs is comparable in power to the CR and SR components. The

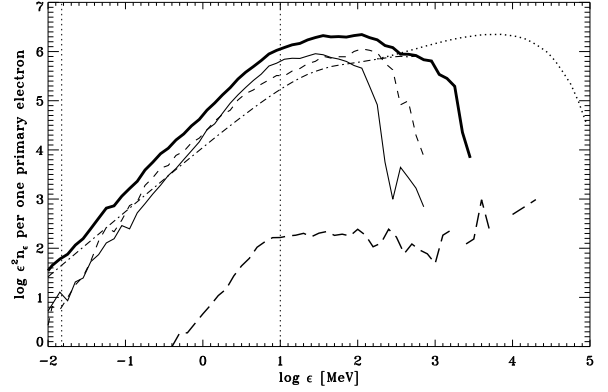


Figure 1. The radiation energy spectrum per logarithmic energy bandwidth due to a single primary electron. The pulsar parameters are  $B_{\text{pc}} = 6 \cdot 10^{12}$  G, and  $P = 0.1$  s and the case **A** ( $R_{\text{hot}} = 10^5$  cm,  $T_{\text{hot}} = 5 \cdot 10^6$  K) is considered. The spectrum consists of four components: the curvature radiation (dot-dashed) and the ICS (long dashed) are due to the primary electron, while the synchrotron radiation (short dashed) and the ICS (thin solid) are due to the secondary  $e^\pm$  pairs. Thick solid line indicates superposition of the CR, the SR and the  $e^\pm$  ICS components. The absorbed part of the curvature spectrum is marked with dotted line. The dotted verticals mark the energy range of IBIS.

secondary  $e^\pm$  pairs do not accelerate and remain in resonance until they lose most of their energy via resonant scatterings.

The  $e^\pm$ -ICS component (thin solid line in Fig. 1) has a well-known shape worked out analytically by Dermer (1990) for the ‘thick target’ regime of the ICS ie. for the case when scatterings considerably decrease the energy of the scattering particle. It resembles a broken power law with the break located at  $\epsilon_{\text{br}}^{\text{ICS}} \simeq B_{12}^2/T_6$  MeV, where  $B_{12} = B/(10^{12}$  G) and  $T_6 = T/(10^6$  K). Below the break the photon index  $\alpha_{\text{ICS}}$  assumes the value close to 0, while above the break  $\alpha_{\text{ICS}} \simeq -2$  (it is the same as for the energy distribution of the ICS emitting pairs, cf. Daugherty & Harding, 1989; Dermer, 1990). The shape of the synchrotron component is somewhat more complicated (see Rudak & Dyks (1999) for detailed analysis), nevertheless its level lowers considerably below the blueshifted cyclotron energy  $\epsilon_{\text{ct}} \simeq \epsilon_B \gamma_{\parallel} \sim 3$  MeV  $(P/(0.1 \text{ s}))^{1/2} (B_{\text{pc}}/\text{TG})$  (Rudak & Dyks, 1999; Harding & Daugherty, 1999). With the CR break at  $\sim 10^2$  MeV (Rudak & Dyks, 1999), most of the power contained in all these spectral components in the case shown in Fig. 1 is confined to the energy range above  $\sim 10$  MeV.

This paucity of power in hard X-ray/soft gamma-ray range, clearly visible in Fig.1, stays in disagreement with observed spectra of high- $B$  (ie. classical) pulsars (note the extreme case of the Crab pulsar with a comparable energy output within soft X-ray and hard gamma-ray window, Thompson et al., 1997).

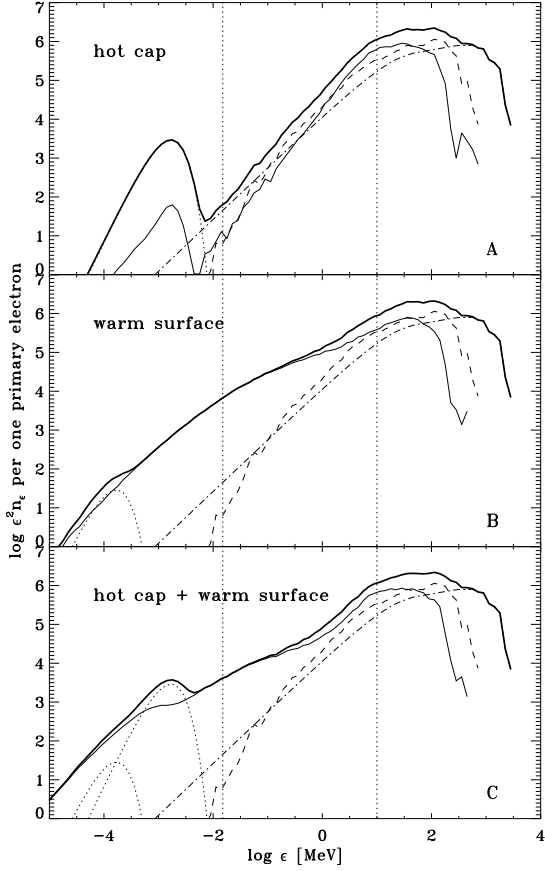


Figure 2. The radiation energy spectra per logarithmic energy bandwidth for three cases of the thermal photon source mentioned in the text: **A** - the hot cap with  $R_{\text{hot}} = 10^5$  cm and  $T_{\text{hot}} = 5 \cdot 10^6$  K; **B** - the entire surface at  $T_{\text{surf}} = 5 \cdot 10^5$  K; **C** - the hot cap of **A** with the rest of the surface at  $T = 5 \cdot 10^5$  K. In all cases  $B_{\text{pc}} = 6 \cdot 10^{12}$  G and  $P = 0.1$  s. The dot-dashed line is for the curvature component, the dashed line is the synchrotron component and the thin solid line denotes the inverse Compton spectrum of photons scattered by the  $e^\pm$  pairs. Dotted line presents contribution of thermal radiation from the surface. Thick solid line is the total spectrum per single primary electron.

In order to increase the spectrum level in this range we will proceed with three different modifications of the case presented in Fig.1.

First, we will change the size and temperature of the soft-photon source, ie. we will consider the cases **B** and **C**. In Fig. 2 the spectrum of Fig. 1 is presented with more details (note the wider energy range) in the upper panel and compared with two spectra calculated for case **B** (the middle panel) and case **C** (the lower panel). The dotted lines in Fig. 2 present the blackbody spectrum of the thermal photon source. Its normalization was estimated in an approximate way described elsewhere (Rudak & Dyks (2001), in preparation). The other lines have the same meaning as in Fig. 1. Note that the ICS component for the warm surface case (thin solid line in the middle panel) extends well into the X-ray regime and at

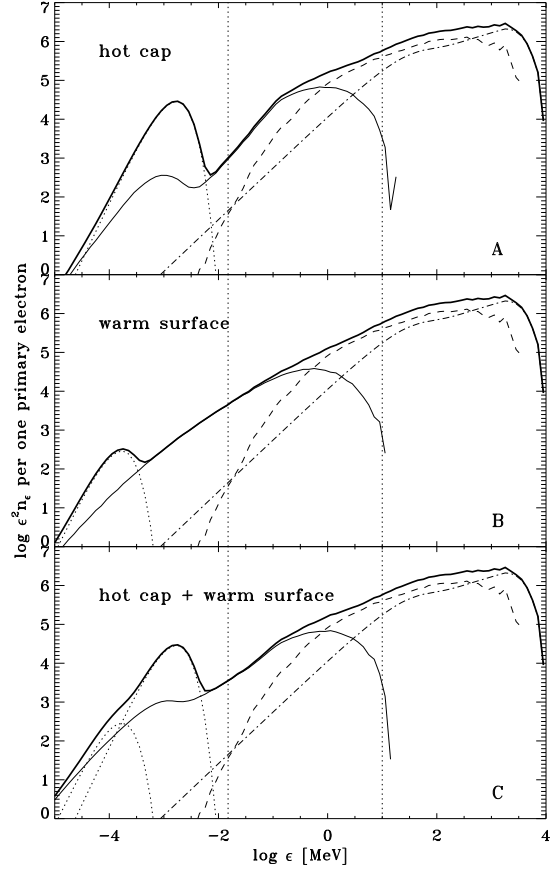


Figure 3. The radiation energy spectra per logarithmic energy bandwidth for the same cases of the thermal photon source as in Fig. 2 but for  $B_{\text{pc}} = 0.6 \cdot 10^{12}$  G and  $P = 0.1$  s. The meaning of all lines is the same as in Fig. 2.

10 keV its level exceeds by two orders of magnitude a level of the spectrum for the hot cap case (upper panel). It has no longer a single power-law shape. The significant difference between the shape of the ICS component for the hot cap case (upper panel in Fig. 2) and the warm surface case (middle panel) comes from a difference between the energy loss rates of electrons in these two cases. The energy-loss-scale-length  $\lambda_\gamma$  is at the resonance of the order of  $10^2$  cm and  $10^4$  cm in the two cases, respectively. In the hot cap case (**A**) electrons lose most energy over a very short distance from the creation point and then leave the resonance regime. In the warm surface case the pairs lose energy in a much slower rate and fulfill the resonant condition over the substantially longer length scale. Because of the larger size of the thermal photon source (the entire surface) they can still scatter resonantly even at a few stellar radii above the surface where the soft tail of the ICS component is produced. When both the hot cap and the rest of surface emit thermal X-ray photons, then both the break at  $\epsilon_{\text{br}}^{\text{ICS}}$  and the soft tail are present in the ICS component of the spectrum (the case shown in the lower panel of Fig. 2).

Second, we can force the spectrum to extend towards lower energies by either lowering the strength of  $B_{\text{pc}}$

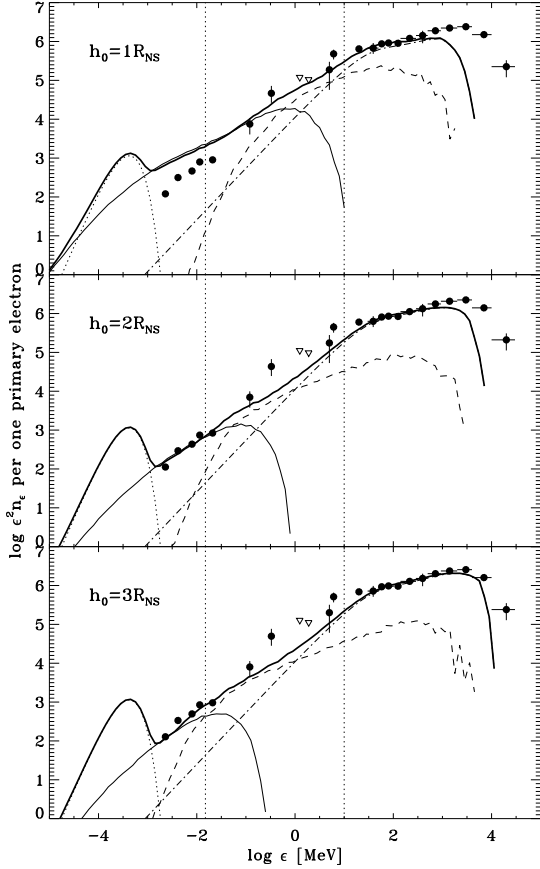


Figure 4. The radiation energy spectra of the Vela pulsar ( $B_{\text{pc}} = 6 \cdot 10^{12}$  G,  $P = 89$  ms,  $T_{\text{surf}} = 1.26 \cdot 10^6$  K). Three panels correspond to different altitudes of a lower boundary of acceleration zone:  $h_0 = 1, 2,$  and  $3 R_{\text{NS}}$  above the surface. The meaning of all lines is the same as in Fig. 2. Filled dots (some with error bars) present data from RXTE, OSSE, COMPTEL and EGRET (Thompson et al. (1997), Strickman et al. (1999)). Triangles denote OSSE and COMPTEL upper limits.

at the polar cap or elevating the accelerator to some high altitude ( $h_0 > 0$ ) to lower the local magnetic field strength. The latter case is justified by the idea of the high altitude accelerator as introduced and argued for by Harding & Muslimov (1998). It is the  $e^\pm$ -ICS component which reacts in this desirable way when the strength of  $B$  decreases: this component extends towards lower photon energies faster than the SR component ( $\varepsilon_{\text{br}}^{\text{ICS}} \propto B^2/T$  whereas  $\varepsilon_{\text{ct}} \propto B$ ).

Let us lower the magnetic field strength at the polar cap by one order of magnitude:  $B_{\text{pc}} = 0.6 \cdot 10^{12}$  G. The spectra for the cases **A**, **B** and **C** are now presented in Fig. 3. In accord with the relation  $\varepsilon_{\text{br}}^{\text{ICS}} \propto B^2/T$ , the ICS component is shifted towards the lower photon energy by two orders of magnitude and dominates for  $\varepsilon \lesssim 1$  MeV. Again, the break at  $\varepsilon_{\text{br}}^{\text{ICS}}$  is present for the hot cap case ( $T = 5 \cdot 10^6$  K, upper panel) and there is a soft tail and no sign of the break for the warm surface case ( $T = 5 \cdot 10^5$  K). The level of the  $e^\pm$ -ICS component for  $B_{\text{pc}} = 0.6 \cdot 10^{12}$  G is one order of magnitude lower than the correspond-

ing level for  $B_{\text{pc}} = 6 \cdot 10^{12}$  G. We emphasize that the main reason for this effect is not a low value of the energy loss rate due to the ICS in weak magnetic fields (in *both* cases the pairs lose almost 100% of energy due to scatterings) but the smaller total energy content of the  $\gamma_{\parallel} mc^2$  distribution for cascade pairs in the low- $B$  case (cf. Zhang & Harding, 2000). This is also the main reason for which the  $e^\pm$ -ICS component is negligible for millisecond pulsars (ie. the photon index predicted for the INTEGRAL range is that of synchrotron component:  $\alpha_{\text{SR}} = -1.5$ , Rudak & Dyks (1999)).

Fig. 4 is to illustrate the case of elevating the accelerator to some high altitude. Three subcases, with  $h_0 = 1, 2,$  and  $3 R_{\text{NS}}$  were considered. Moreover, the figure enables the comparison of the model predictions with the data for the Vela pulsar, coming from the compilation by Thompson et al. (1997) and Strickman et al. (1999). The spectra were calculated for the entire surface at  $T_{\text{surf}} = 1.26 \cdot 10^6$  K (Ögelman, 1995). In spite of large altitudes at which the  $e^\pm$  pairs are created (low  $B$ ), the  $e^\pm$  ICS component contributes considerably within the X-ray range and improves agreement between the theory and the data.

#### ACKNOWLEDGMENTS

This work was supported by KBN grant 2P03D 02117.

#### REFERENCES

- Daugherty J.K., Harding A.K., 1982, ApJ 252, 337
- Daugherty J.K., Harding A.K., 1989, ApJ 336, 861
- Dermer C.D., 1990, ApJ 360, 197
- Dyks J., Rudak B., 2000, A&A 360, 263
- Harding A.K., Daugherty J.K., 1999, Astrophysical Letters & Communications 38, 25
- Harding A.K., Muslimov A.G., 1998, ApJ 508, 328
- Ögelman H.: 1995, X-Ray Observations of Cooling Neutron Stars. In: The Lives of the Neutron Stars, Alpar M.A., et al. (eds.), Kluwer, 101
- Rudak B., Dyks J., 1999, MNRAS 303, 477
- Strickman M.S., Harding A.K., deJager O.C., 1999, ApJ 524, 373
- Thompson D.J., Harding A.K., Hermsen W., Ulmer M.P., 1997, In Proc. of the 4th Compton Symposium, Dermer C.D., Strickman M.S., Kurfess J.D. (eds.), AIP 410, New York, 39
- Zhang B., Harding A.K., 2000, ApJ 532, 1150